JOURNAL OF MAGNETIC RESONANCE **127,** 73–79 (1997)
ARTICLE NO. MN971172

A Solenoid-Like Coil Producing Transverse RF Fields for MR Imaging

E.-K. Jeong,*,† D.-H. Kim,‡ M.-J. Kim,* S.-H. Lee,‡ J.-S. Suh,* and Y.-K. Kwon§

*Department of Diagnostic Radiology and ‡Department of Physics, Yonsei University, Seoul, South Korea; and §Applied Superconductivity Laboratory, Korean Electrotechnology Research Institute, South Korea

Received October 22, 1996; revised March 24, 1997

A solenoidal RF coil is presented that generates an RF field only perpendicular to the long axis, so that it can be used longitudinally in the usual superconducting solenoid magnet for NMR. This new design is superior to the traditional saddle coil or Helmholtz pair. Applications for the coil will include imaging of legs, arms, etc., as well as analytical application in high-resolution NMR. A tilted single-turn-solenoid, which has the plane of each loop tilted with respect to the cylinder axis, is implemented to generate an RF field with a component perpendicular to the coil-cylinder axis. The novel addition of an eddy-current coil eliminates the undesirable longitudinal component of the RF field, leaving an RF field entirely perpendicular to the coil-cylinder axis. By inserting the eddy coil, the spatial homogeneity of the transverse RF field is greatly improved, with significant increases in the H_1 field strength and receiving sensitivity. Images with the eddy-coil-modified tilted solenoid are remarkably uniform in intensity over a large useful volume.

INTRODUCTION

The RF coil plays an important part in NMR as the antenna for coupling between the electronics and the nuclear spin system of interest. Only the component of the RF field that is orthogonal to the static magnetic field is effective in obtaining the NMR signal. Easy access of the subject into the coil and the spatial homogeneity of the RF field are also very important for MR imaging (*1–3*).

Most MR imaging systems use a superconducting magnet with the magnetic field almost universally along the cylindrical axis, which is also the usual access direction of the human subject. The solenoid RF coil is known to give good spatial homogeneity of the field and to have a high efficiency compared to other coils (4), but because the RF field inside the standard solenoid coil is parallel to the cylinder axis, the solenoid must be oriented nearly perpendicular to the main field. This orientation is obviously difficult or impossible for patient access, and this is the main reason the solenoid RF coil has not been widely used for MR imaging of humans. Modified versions of the solenoid using a single turn have been intensively studied by Hornak (*5–7*), but these coils lack homogeneity around the perforation and offer difficult access for the patient.

A component of the RF field ($H_1 \sin \psi$) can be generated *perpendicular* to the cylindrical axis of the solenoid coil by tilting each current loop from the cylinder axis by angle ψ, as shown in Fig. 1. This tilted solenoid coil has been applied in solid-state NMR experiments in a superconducting magnet. A significant amount of NMR signal was detected due to fringe fields (*8*), even with the cylinder axis of the coil parallel to the $\mathbf{H}_0$ field.

We modified the tilted solenoid coil by forming a single-turn version (TSTS) (*9, 10*). Since the longitudinal component does nothing for manipulating spins but depositing RF energy into the subject as heat, we have now developed a method using eddy currents to eliminate the RF field component along the cylinder axis so that the resultant RF field has only a transverse RF magnetic field, perpendicular to the cylinder axis. We call this a TSTS coil utilizing eddy currents (ETSTS); it has a longer $\mathbf{H}_1$ for a given power (or less power for given $\mathbf{H}_1$) and greater receiving sensitivity, compared to a TSTS without the eddy-current coil. The $\mathbf{H}_1$/ sensitivity distribution is also remarkably uniform over a large volume.

EXPERIMENTAL

Construction of ETSTS

An ETSTS coil is a composite of two solenoids as in Fig. 1. One is a TSTS, which generates an RF field perpendicular to the current loops, tilted from its coil-cylinder axis. The other is the eddy coil which has a 0° tilt angle and eliminates the longitudinal portion of the field from the TSTS coil.

One TSTS coil with a 10 cm effective length (30 cm total length) and a 10 cm coil diameter was constructed (TSTS10). Later, ETSTS10 was constructed from TSTS10 by inserting an eddy coil, reducing the available inner diameter to 9.4 cm. These coils were used for the comparison study of the spatial homogeneity and the efficiency of the RF field. ETSTS for arm and hand imaging had a 10 cm diameter and a 15 cm effective length (named ETSTS

† To whom correspondence should be addressed.

1090-7807/97 $25.00

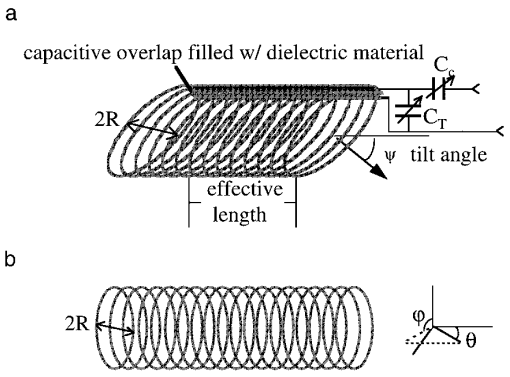

FIG. 1. Construction of the ETSTS coil. Shaded areas represent the ribs (current path) of the coil. The longitudinal component of the RF field generated by the TSTS is eliminated by the eddy coil, which is inserted into the TSTS coil. R is the radius of the eddy coil or half the minor axis of the elliptic loop of the TSTS.

[arm]), and that for leg imaging had a 15 cm diameter and a 20 cm effective length (named ETSTS[leg]). The tilt angle was 45° for all tilted coils. The dimensions and the measured Q values for some coils are listed in Table 1.

Tilted single-turn solenoid. A number of TSTS resonators were constructed from 3M copper tapes (3M, U.S.A.). When a TSTS was spread out, the tapes form cosine curves as shown in Fig. 2. The amplitude and the wavelength of the cosine curve are R tan ψ and $2\pi R$, respectively. Here, R is the radius of the coil cylinder (or half the minor axis of the elliptic loops of the TSTS coil) and ψ is the tilt angle, respectively. For example, the 10 cm o.d. cylindrical TSTS with $\psi = 45°$ had amplitude $A = 5$ cm and wavelength $\lambda = 31.4$ cm. A wide copper tape was attached to a large polyethylene film. A cosine curve with proper wavelength and amplitude was printed onto a large paper sheet and was then pasted onto a thick paper support to be used as a guide for drawing all the ribs onto the copper film as shown in Fig. 2. Then the spaces between the ribs were cut and peeled off. We chose 2 mm for both the width of the ribs and the spacing between the ribs. The width of the ribs must be relatively narrow to reduce the capacitive coupling between the ribs and the sample. The numbers of the individual loops of TSTS varied depending upon the length of the coil.

One centimeter-wide transverse strips were left at the three extrema of the cosine curves. When the cylinder was formed, the strips at the ends overlapped with a thin polyethylene film between the strips as the dielectric material, making a long and evenly distributed capacitor to provide a resonator (*9*). The capacitance was varied by adjusting the area and the thickness of the dielectric material in the overlap.

The copper film containing the ribs were wound around a Plexiglas cylinder, each rib making an oblique ellipse with the tilt angle ψ to the coil-cylinder axis. Thus, the current running through the oblique ribs generated the RF magnetic field tilted from the cylinder axis by an angle ψ (*8, 12, 13*). The total length of a TSTS coil was the sum of the effective length and $4R$ tan ψ. Thus, for a tilt of 45°, the total length is the sum of the effective length and $4R$.

Even though the coarse tuning was accomplished by adjusting the thickness and the area of the dielectric material between the capacitor strips, it was convenient to have capacitive fine tuning and matching to 50 Ω (see Fig. 1). The range of the tuning capacitance was about 50–100 pF for ETSTS10 and TSTS10 coils. A small nonmagnetic capacitor with a nominal breakdown voltage of 500 V was added for fine tuning in parallel to the TSTS. The matching of the coil to 50 Ω was accomplished by using another capacitor in series. There was never any RF breakdown problem with this scheme for peak transmitter powers of 1000 W.

Eddy coil. Another assembly of ribs with tilt angle 0° (=eddy coil) was constructed for the ETSTS coil. Instead of making many cosine curves as for a TSTS coil, the eddy coil only requires straight lines and the ends are soldered together to make complete loops. The eddy coil is either inserted into or overlapped onto the TSTS as in Fig. 1. This coil does not have direct connection to the system (it floats electrically), interacting with the main tilted coil via mutual

TABLE 1
Overall Specifications of TSTS and ETSTS Coils Constructed for This Study

Coils	Diameter (cm)	Effective length (cm)	Total length (cm)	Un-/loaded Q	Anatomy
TSTS10	10	10	30	70/27[a]	
ESTS10[b]	10	10	30	66/33[a]	
ETSTS[arm]	10	25	45	65/36[c]	Arm
ETSTS[leg]	15	18	48	67/38[c]	Leg

Note. Tilt angles for all coils are 45° with respect to the coil-cylinder axis.
[a] 1000 cc of saline phantom was used for loading the coils.
[b] TSTS10 coil was used for the construction of ETSTS10.
[c] 2000 cc of saline phantom was used for loading the coils.

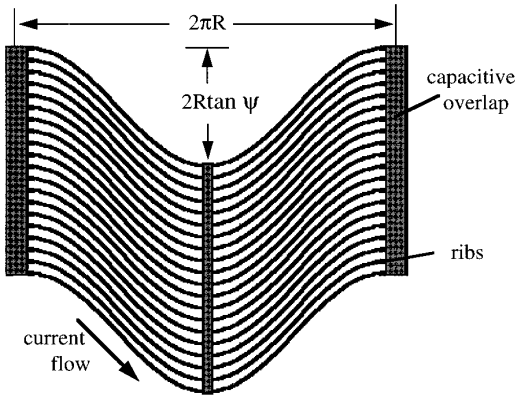

FIG. 2. Planar configuration of the current-carrying loops before they are wrapped around the support cylinder to form the solenoid. Each current loop follows the cosine curve when it is spread out, with its amplitude R tan ψ and wavelength $2\pi R$. The wide stripes at both ends were used as capacitive overlap for tuning.

induction and generating eddy currents to cancel the time-varying field along the cylinder axis (*11, 12*).

Evaluation of Coils

A constant RF source (sine wave) was applied to the ETSTS[leg] (15 cm o.d.), and the intensity of the RF field generated in the coil was measured by direct measurement of the induced EMF with a small nonresonant pickup coil (10 mm long, 5 mm diameter, 10 turns) (*14*). The pickup coil was placed in various locations along the center axis and oriented at various polar and azimuthal angles at the coil center. The RF field ($\mathbf{H}_1$) map may also be calculated using a spin-echo image (*14*).

The phantom used for the homogeneity study was 1000 cc of saline in a plastic bottle (6.5 cm o.d./18 cm long). Approximately 0.63 mmol of Gd-DTPA was added to decrease the water ^{1}H T_1 to 900 ms. The homogeneity and the efficiency of the ETSTS coil were evaluated for coil ETSTS10. It had an effective length of 10 cm, access diameter of 9.4 cm, and a total length of 30 cm. The same phantom was imaged with a GE linear extremity coil (birdcage type), with the same scanning parameters as those for ETSTS10.

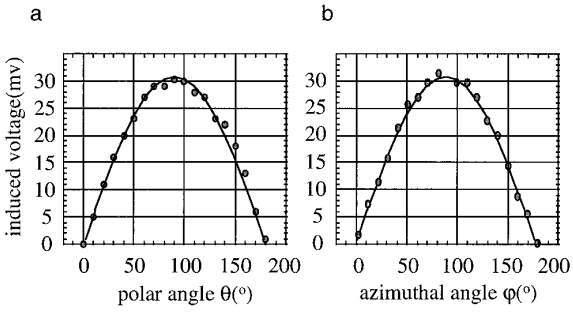

FIG. 3. Plots of the induced voltage on a small nonresonant pickup coil, with respect to (a) the azimuthal angle φ with $\theta = 90°$, and (b) the polar angle θ with $\varphi = 90°$ at the center of the leg version of the ETSTS.

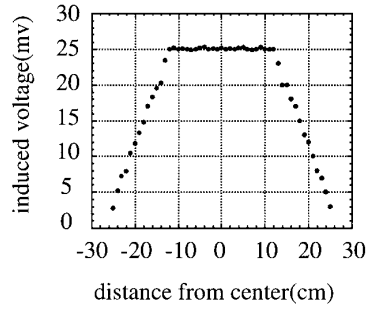

FIG. 4. Plot of the induced voltage along the center axis of the leg version of the ETSTS. The horizontal axis represents the distance from the center of the coil in centimeters.

The ETSTS coil was connected to a clinical MRI machine, GE Signa 1.5 T (General Electric Medical Systems, Milwaukee, Wisconsin), using a GE linear extremity coil adapter. The RF input to the RF power amplifier was attenuated just before the input port of the RF amplifier, and the amount of the attenuation depended upon the size of the coil (e.g., −6 dB for ETSTS10).

ETSTS[arm] and ETSTS[leg] coils were used for getting MR images of hand and leg of a healthy volunteer and compared with those using a GE linear extremity (knee) coil. Images of the hand using the knee coil were obtained with the subject in a prone position, and the remaining images with the subject in a supine position. No quantitative analyses on the human images were pursued; only a visual examination was performed.

RESULTS AND DISCUSSION

The unloaded Q and the loaded Q (for the saline phantom) values of selected coils are listed in Table 1. There was

TABLE 2
Evaluation of MR Images Obtained with TSTS10 and ETSTS10 Coils

Coils	Transmitter gain (dB)[a]	SNR
TSTS10	7.6	192
ETSTS10	4.0	283
GE extremity	3.9	253

Note. The SNR of TSTS was measured near the obtuse corner of the TSTS, which gave the maximum signal intensity (see where the arrows point in Fig. 5a). The signal intensity for the GE coil was measured near the center of the phantom image.

[a] Relative RF power required for nutating the magnetization by 90° for fixed pulse duration.

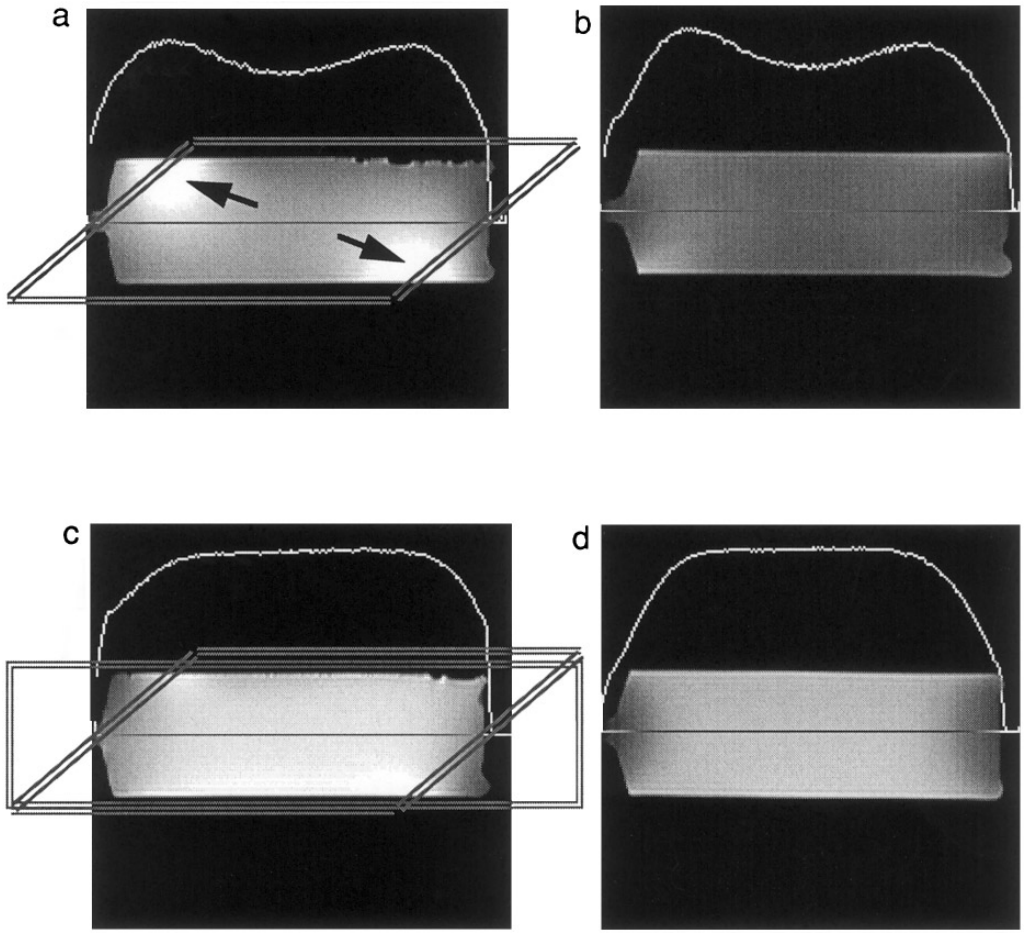

FIG. 5. Spin-echo images of the saline phantom obtained using TSTS10 and ETSTS10 coils with TR/TE = 400/14 ms. Parallelograms in (a) and (c) show the relative sizes and locations of the coils with respect to the phantom while being imaged.

little difference in the loaded and unloaded Q values of the ETSTS10 and TSTS10 coils. Two megahertz of tuning range was easily obtained with 45 pF of tuning capacitance C_T for TSTS10/ETSTS10 coil. The 50 Ω matching of the coil assembly was obtained by adjusting the coupling capacitor C_C with about 100 pF range. The number of individual loops varied depending upon the length of the coils. For our choice with 2 mm width and gap of ribs, the number of current loops of ETSTS10 was 50 and 75 for the TSTS and eddy coil, respectively.

Figures 3a and 3b are plots of the induced EMF in the pickup coil versus the polar angle θ and the azimuthal angle φ, respectively, in arbitrary units, measured at the center of the 15 cm o.d. ETSTS (see Fig. 1 for the definitions of angles θ and φ). The maximum EMF is measured with the pickup coil in the transverse plane $\theta = 90°$ as in the plot of Fig. 3a. It implies that the RF field is perpendicular to the cylinder axis as expected. The maximum EMF was also measured when the pickup coil axis was along the major axis of the ellipse (tilted circle), with the azimuthal angle $\varphi = 90°$ as in the plot of Fig. 3b. Sine curves are drawn in Figs. 3a and 3b as solid lines to show how well the measured data fit Faraday's law of induction. These results imply that $\mathbf{H}_1$ is perpendicular to the cylinder axis.

The induced voltage with the pickup coil positioned perpendicular to the cylinder axis is plotted in Fig. 4 for the coil ETSTS[leg] (15 cm o.d.). The RF field strength is very uniform along 120% of the effective length. These data were obtained along the center axis of the coil cylinder with the polar angle $\theta = 90°$ and the azimuthal angle $\varphi = 90°$, the angles for which the transverse RF field is a maximum. The field plot along off-center lines was not examined. Nor did this method of measuring the RF field inside the coil take into account the sample loading effect. Nevertheless this plot and those of Fig. 3 demonstrate the superb spatial homogeneity and the direction of the RF field inside the coil assembly.

The effect of the floating eddy coil was evaluated with TSTS10 and ETSTS10 coils, which had the same physical dimensions. First, the TSTS coil with 10 cm o.d. and 10 cm effective length was constructed on a Plexiglas tube (10 cm

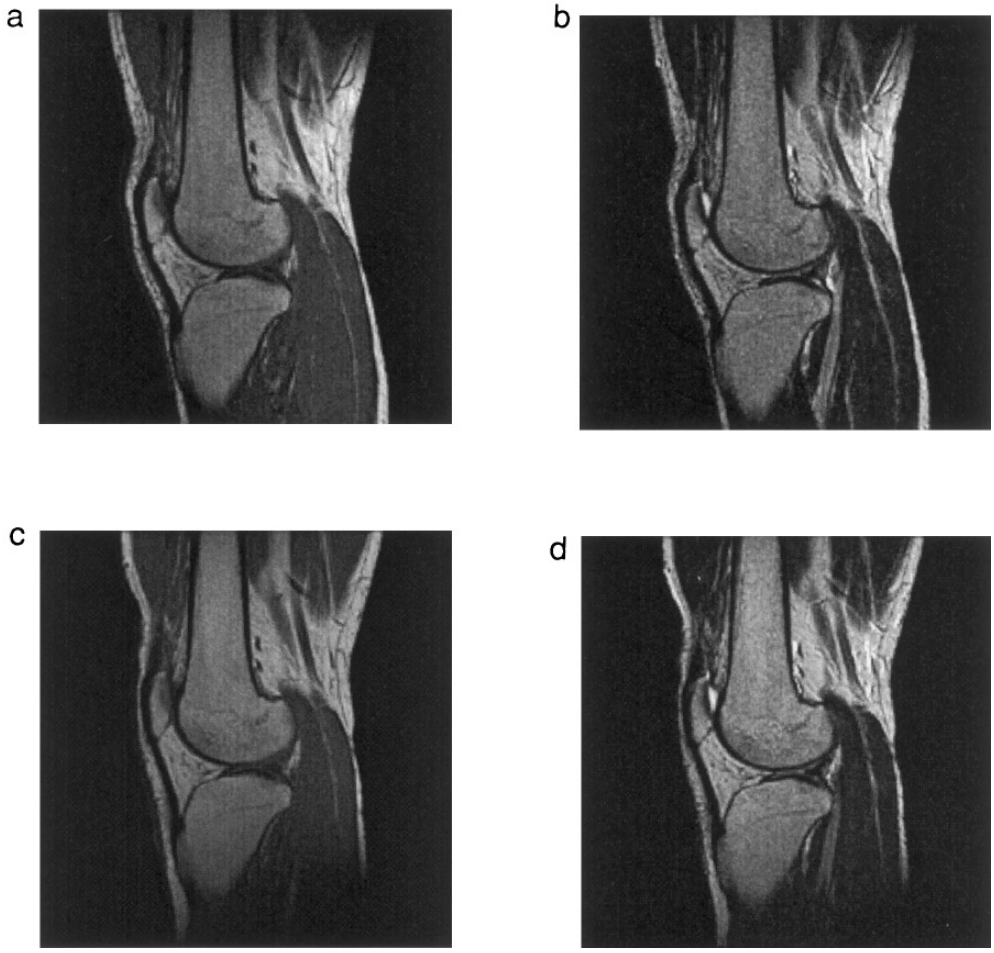

FIG. 6. T_1- and T_2-weighted images taken with the coil ETSTS(leg] (a, b) and with the GE knee coil (c, d). Images (a, c) are T_1-weighted images obtained with TR/TE = 400/14 ms and spin-echo pulse sequence, and (c, d) are T_2-weighted with TR/TE of 2500/95 ms, 16 ETL, and fast spin-echo pulse sequence. Field-of-view (FOV) was 16 cm for all images.

o.d./3 mm thick) and tuned to 63.87 MHz (TSTS10), and the characteristics such as loaded/unloaded Q values and MR imaging of a phantom were evaluated. The ETSTS10 was then constructed by inserting the eddy coil into the TSTS10 and retuning to the NMR frequency, and evaluated. The resonance frequency of the coil assembly increased by several tens of megahertz on inserting an eddy coil into the TSTS.

The $\mathbf{H}_1$ performances and the receiving sensitivities of TSTS10 and ETSTS10 were examined by imaging the saline phantom. The spin-echo pulse sequence was used for obtaining most of the images. The common scanning parameters were 400/14 ms TR/TE, 1 NEX, 256 $\times$ 128 matrix, and 5 mm slice thickness. The field-of-view for the coronal and sagittal MR images was 20 cm. T_2-weighted images of the leg were obtained using a fast spin-echo (FSE) pulse sequence with 16-echo train length (ETL) and 16 kHz receiver bandwidth.

The transmitter gains (TG), representing the required RF power to make a 90° flip of the magnetization for a fixed pulse duration (3.2 ms-long slice-selective sinc pulse), were recorded for each coil from the scanner. First, TSTS10 was examined with the saline phantom. Then after inserting the eddy coil and retuning ETSTS10, the MR images of the same phantom for the ETSTS10 were obtained with the same scanning parameters as for the TSTS10 coil.

ETSTS10 required 3.6 dB less transmitter gain than the TSTS10 for the same scanning parameters and the same phantom, as indicated in Table 2. Thus, more transverse $\mathbf{H}_1$ is generated in ETSTS10 than in TSTS10 for the same RF input power. This means the RF performance is improved by inserting the eddy coil into the TSTS. Power increase of 3.6 dB for TSTS means more power dissipated into the subject. Data for the GE linear extremity coil were measured using the same scanning parameters and the same phantom as those for ETSTS10. The inner volume of coils were different for the GE extremity coil (17 cm diameter and 28 cm length) and TSTS10/ETSTS10.

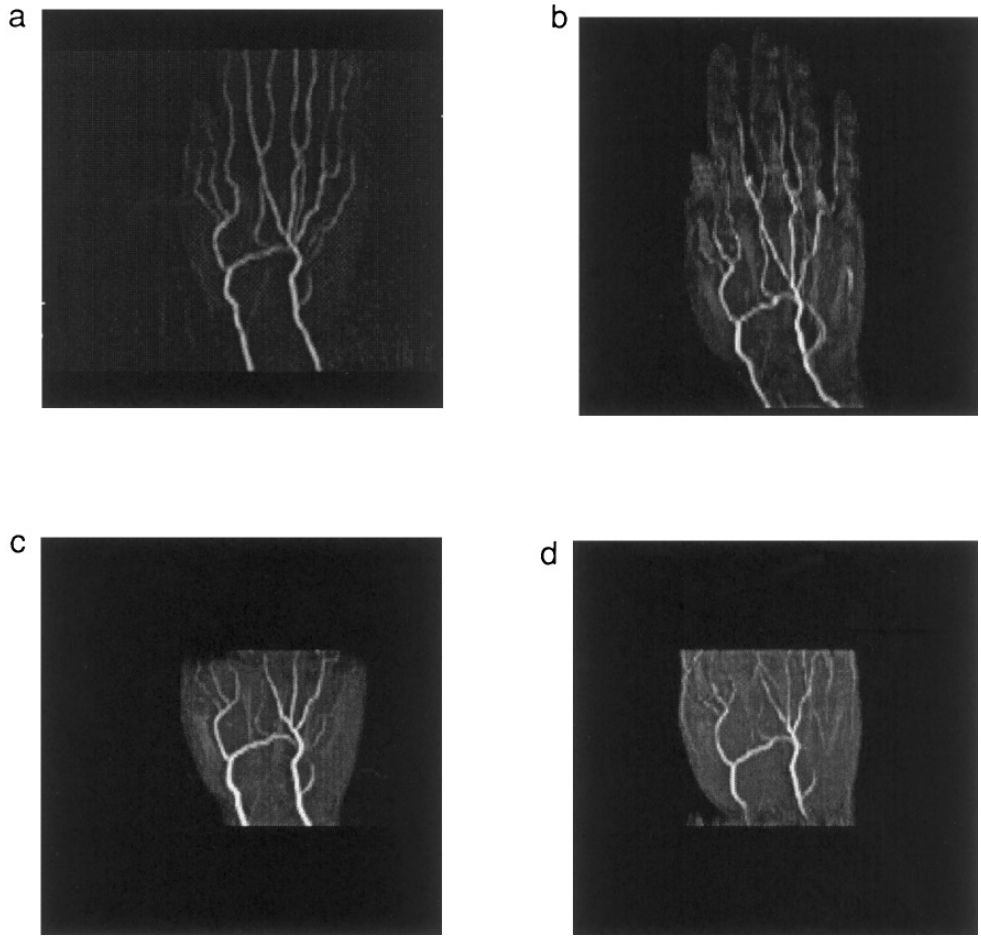

FIG. 7. Two- (a, b) and three-dimensional (c, d) TOF MR angiograms of a normal volunteer. Images (a, c) were obtained using ETSTS[arm] in supine position, and (b, d) using the GE knee coil in prone position.

The MR image with ETSTS10 coil gave about 1.47 times more SNR than TSTS10 as shown in Table 2. This is an about 3.3 dB increase, which is close to 3.6 dB of TG difference between them. Since their Q values are almost the same and the same scanning parameters and phantom were used for imaging, this 3.3 dB increase must come from the difference between the two coils' transverse components of $\mathbf{H}_1$, as shown in the difference in their TG values.

The images of Fig. 5 are the sagittal and coronal slices of the saline phantom in TSTS10 (5a, 5b) and ETSTS10 (5c, 5d). The schematic drawings of the coils, used for imaging, are overlaid on Figs. 5a and 5c. The parallelograms in images 5a and 5c represent the TSTS coil, and the rectangle in Fig. 5c is the eddy coil of ETSTS10. The signal intensities along the center line of each image are plotted on the image. The image using the TSTS coil has high intensity near the obtuse corners of the parallelogram, where the arrows point in Fig. 5a, and the signal intensity is much higher around both ends of the coils. In contrast, ETSTS gave much more uniform signal intensities inside the coil volume.

Figures 6a and 6b are spin-echo images of a normal volunteer using a leg ETSTS coil. For comparison, images using a conventional knee coil are displayed in Figs. 6c and 6d. The T_2-weighted images (Figs. 6b, 6d) were obtained using a fast spin-echo (FSE) sequence with 16-echo train length and 16 kHz receiver bandwidth. Although the centers of the images were not placed at the exact center of the most homogeneous coil volumes, our homemade ETSTS coils qualitatively gave more or, at least, comparably homogeneous MR signal intensity than those of the knee coil, as seen in the intensity of the subcutaneous fat. The authors mean to give no direct comparison of the two coils, since the sensitive imaging volumes of the two coils are different because of their different sizes.

Two- (Figs. 7a, 7b) and three-dimensional (Figs. 7c, 7d) TOF MR angiograms of the arteries of one of our hands were obtained with ETSTS[arm] (Figs. 7a, 7c), and compared to those of the GE knee coil (Figs. 7b, 7d). MR images of the hand were taken in the supine position for the ETSTS coil, while those using the knee coil were obtained in the prone position. The discomfort for hand imaging was greatly re-

duced by using the ETSTS coil. The scanning parameters for the imaging of the hand with ETSTS were identical to those for the conventional knee coil. The signal intensities on the images of ETSTS coil are more uniform throughout the hand than those of the conventional knee coil. Although the uniformity of the signal intensity in the imaging volume may not be very useful, it helps for the quantitative or the comparative evaluation of different regions in the image. The distal arteries in Fig. 7a are as clearly visible as is the proximal artery, while the distal arteries rapidly degraded with the knee coil.

CONCLUSION

The tilted solenoid RF coil was implemented for MR imaging. A solenoid with the turns connected in parallel was used to reduce the inductance of the main coil (*11*, *12*). We corrected the tilted solenoid coil with the eddy coil, eliminating the longitudinal component of the $\mathbf{H}_1$ generated by the tilted solenoid.

Adding an eddy coil gave two benefits to the TSTS coil. One was the great improvement of the spatial RF homogeneity. The other was improved $\mathbf{H}_1$ (3.6 dB), resulting in improved receiving sensitivity (3.3 dB) and the reduction of RF power deposition compared to that of the TSTS coil with the same subject.

ACKNOWLEDGMENTS

This work was supported partly by a fund from Korean Electrotechnology Research Institute, a grant from Yonsei University, and Basic Science Research Institute Program from Korean Ministry of Education (KOSEF through SPRC, 1996, Project 2424). The authors thank Drs. M. S. Conradi and E. Fukushima for helpful discussions.

REFERENCES

1. E. Fukushima and S. B. W. Roeder, ''Experimental Pulsed NMR: A Nuts and Bolts Approach,'' Addison-Wesley, Reading, Massachusetts, 1981.
2. C. P. Slichter, ''Principles of Magnetic Resonance,'' Springer-Verlag, Berlin, 1990.
3. P. G. Morris, ''Nuclear Magnetic Resonance Imaging in Medicine and Biology,'' Oxford Univ. Press, London, 1986.
4. D. I. Hoult and R. E. Richards, *J. Magn. Reson.* **24,** 71 (1976).
5. J. P. Hornak, E. A. Marshall, J. Szumowski, and R. G. Bryant, *Magn. Reson. Med.* **7,** 442 (1988).
6. E. A. Marshall, J. J. Listinsky, T. L. Ceckler, J. Szumowski, R. G. Bryant, and J. P. Hornak, *Magn. Reson. Med.* **9,** 369 (1989).
7. S. D. Szeglowski and J. P. Hornak, *Magn. Reson. Med.* **30,** 750 (1993).
8. Y. Sun and G. E. Maciel, *J. Magn. Reson. A* **105,** 145 (1993).
9. M. F. Koskinnen and K. R. Metz, *J. Magn. Reson.* **98,** 576 (1992).
10. P. L. Kuhns, M. J. Lizak, S.-H. Lee, and M. S. Conradi, *J. Magn. Reson.* **78,** 69 (1988).
11. J. D. Jackson, ''Classical Electrodynamics,'' Wiley, New York, 1975.
12. J. R. Reitz and F. J. Milford, ''Foundations of Electromagnetic Theory,'' Addison-Wesley, New York, 1978.
13. D. I. Hoult and P. C. Lauterbur, *J. Magn. Reson.* **34,** 425 (1979).
14. J. P. Hornak, J. Szumowski, and R. G. Bryant, *Magn. Reson. Med.* **6,** 158 (1988).